

Shape Classification of the Anterior Cruciate Ligament Cross Section

by

Michael A. DiNenna

B.S. Physics, University of Florida, 2018

B.A. Astronomy, University of Florida, 2018

Submitted to the Graduate Faculty of the
Swanson School of Engineering in partial fulfillment
of the requirements for the degree of
Master of Science in Mechanical Engineering

University of Pittsburgh

2021

UNIVERSITY OF PITTSBURGH

SWANSON SCHOOL OF ENGINEERING

This thesis was presented

by

Michael A. DiNenna

It was defended on

November 2, 2021

and approved by

Jeen-Shang Lin Sc.D., Associate Professor, Department of Civil and Environmental Engineering

Mark C. Miller Ph.D., Associate Research Professor, Department of Mechanical Engineering and
Materials Science

Qing-Ming Wang Ph.D., Professor, Department of Mechanical Engineering and Materials
Science

Thesis Advisor: Patrick Smolinski Ph.D., Associate Professor, Department of Mechanical
Engineering and Materials Science

Copyright © by Michael A. DiNenna

2021

Shape Classification of the Anterior Cruciate Ligament Cross Section

Michael A. DiNenna, M.S.

University of Pittsburgh, 2021

The objective of this study is to quantifiably classify the shape of the cross section of the anterior cruciate ligament (ACL). This will be done with the use of a three-dimensional laser scanner to construct a solid model and mathematical analysis.

Ten freshly frozen cadaveric knees were used in this study. The intact knees were positioned in a six degrees of freedom robotic testing system. The knee was passively moved by the robot from full extension to 15 degrees flexion. The knee was then dissected so that only the ACL, tibia, and femur remained. The dissected knee was placed in the robot and placed into the same position of 15 degrees of flexion as the intact knee. The ACL was laser scanned and the insertion sites points were discretized. A three-dimensional model was constructed using software. The ligament axis was defined to be the line that connects the centroids of the two insertion sites. Five planes were defined perpendicular to this axis to represent the cross sections. Points outlining each cross section were compared to five shapes (ellipse, rectangle, triangle, peanut shape, and kidney shape) and the fit of the shape was measured using a Procrustes analysis.

Twenty-nine out of the fifty cross sections were found to be best fit to an ellipse. Compared to seven for triangle and kidney shape, five for rectangle, and only two for the peanut shape.

Overall, the ellipse provided the best fit for a plurality of the cross sections. This study may provide information to construct ACL grafts with shapes closer to that of the original tissue.

Table of Contents

Preface.....	ix
1.0 Introduction.....	1
2.0 Background	2
2.1 Anatomical Definitions.....	2
2.2 Procrustes Formula	4
2.2.1 Previous Work with Procrustes Method.....	4
2.2.2 Description of Procrustes Formula.....	5
3.0 Methods.....	9
3.1 Specimen Preparation	9
3.2 Laser Scanning of the Anterior Cruciate Ligament.....	11
3.3 Analysis of Three-Dimensional Computer Model	11
3.3.1 Creating the Solid Model.....	11
3.3.2 Defining the ACL Cross Sectional Axis	11
3.4 Shape Analysis of Ligament Cross Sectional Area.....	12
3.4.1 Processing of the Cross Sectional Data	12
3.4.2 Creating the Shapes	15
3.4.3 Comparing Defined Shapes to the Cross Sectional Area Point Data	22
3.4.4 Analysis of the Data	28
4.0 Results	30
4.1 Best Fit Shape for Individual Cross Sections.....	31
4.2 Best Fit Shape for All Cross Sections	32

4.3 Best Fit Shape by Cross Section for All Specimens.....	32
4.4 Best Fit Shape for One Specimen Amongst All Levels	33
4.5 Mid-Level Cross Section vs Distal and Proximal Cross Sections.....	33
5.0 Discussion.....	34
5.1 Comparison.....	34
5.2 Application	35
5.3 Limitations	36
6.0 Conclusion	37
6.1 Conclusion.....	37
6.2 Future Work	37
Bibliography	38

List of Tables

Table 1: Best Shape in Each Shape and Level	31
Table 2: Best Fits for All Cross Sections.....	31
Table 3: Average Procrustes Distance for All Shapes over All Cross Sections.....	32
Table 4: Best Shape for Each Level.....	32
Table 5: Best Shapes for Each Sample.....	33
Table 6: Comparison of Mid-Level Cross Section vs Proximal and Distal Cross Sections .	33

List of Figures

Figure 1: Knee Anatomy with Labeled Ligaments⁶.....	3
Figure 2: Process of the Procrustes Method in Fitting One Shape to Another¹⁰	4
Figure 3: Dissected Knee so that Only ACL, Tibia, and Femur Remain	10
Figure 4: An Acute Triangle with Labeled Sides and Angles.....	17
Figure 5: An Obtuse Triangle with Labeled Sides and Angles	18
Figure 6: Peanut Shapes with $b = 1.3, 1.4,$ and 2.0 from Left to Right	21
Figure 7: Centered Kidney Shape.	22
Figure 8: Best Fit Ellipse Compared to the Mid-Level of Sample 5 with Procrustes Distance Equal to 0.0019	24
Figure 9: Best Fit Rectangle Compared to Mid-Level of Sample 5 with Procrustes Distance Equal to 0.0129	25
Figure 10: Best Fit Triangle Compared to Mid-Level of Sample 5 with Procrustes Distance Equal to 0.0429	26
Figure 11: Best Fit Peanut Shape Compared to Mid-Level of Sample 5 with Procrustes Distance Equal to 0.0084	27
Figure 12: Best Fit Kidney Shape Compared to Mid-Level of Sample 5 with Procrustes Distance Equal to 0.0097	28

Preface

I would like to thank my thesis advisor Dr. Patrick Smolinski, for pushing me to reach my potential and the encouragement he has given along the way. I would also like to thank Taylor Price, Michael Smolinski, Dr. Tomomasa Nakamura, and Monica Linde for their help in making this project come together. Finally, I dedicate this thesis to my loving wife who always has my back and never gives up on me.

1.0 Introduction

The purpose of this study is to develop methods to quantitatively classify the shape of the cross section of the anterior cruciate ligament (ACL). Around 200,000 ACL injuries occur every year in the United States and roughly half of those are reconstructed.¹ In the past, photographs, calipers, MRIs and laser micrometers were used to measure the cross sectional area of the ACL. Today, three-dimensional laser scanning(Fujimaki et al) is used to measure the cross sectional area (CSA) of the ACL.² Others have used computer imaging to look at the footprint of the ACL and found the mean distance of the posterior and anterior bundle to the center of the ligament.³ Price et al studied the principal second moment of inertia of ACL cross sections.⁴ They found that the ratio of major-to-minor axis length of the cross sections decreased from the femoral insertion site to the tibial insertion site. This study will investigate the classification of the cross sections to five defined shapes. This may, in the future, allow clinicians to construct ACL grafts which are closer in shape to that of the native ACL.

2.0 Background

To grasp the scope of this project, anatomical terms need to be defined as well as the nature of the injury and reconstruction. Likewise, the theory behind the quantitative shape comparison will be presented to understand the methods of the analysis.

2.1 Anatomical Definitions

The human knee is composed of four primary ligaments linking the tibia and femur. These are the anterior cruciate ligament (ACL), the posterior cruciate ligament (PCL), lateral collateral ligament (LCL), and medial collateral ligament (MCL). The ACL and PCL are shown in Figure 1. The main function of the ACL and PCL is to restrict anterior and posterior tibial translation, respectively. The focus of this study will be on the ACL. The ACL connects the femur and tibia and is located at the center of the knee. As previously stated, the ACL is primarily responsible for restricting anterior tibial translation (ATT).⁵ The ACL also plays a role in restricting tibial rotation and valgus and varus bending.⁵



Figure 1: Knee Anatomy with Labeled Ligaments⁶

If the ACL is damaged, it may be surgically reconstructed with a graft formed from a ligament or tendon tissue about 50% of the time.¹ One factor for this is the lifestyle of the patient. If they are an athlete, then they are much more likely have their ACL reconstructed than a non-athlete.¹ The harvested tissue is prepared as a graft which is approximately cylindrical in shape. Anatomical studies of the ACL have been done to obtain information of the size and shape of the ligament.⁷ Harner et al. noted the cross sectional shape of the ACL footprint was “irregular”.⁷ “Irregular” was defined as “neither purely circular or elliptical or any other simple geometric shape”. The “irregular” shape was consistent amongst their eight specimens.

2.2 Procrustes Formula

The Procrustes formula, is a formula that is used to quantify the similarity between two shapes.⁸ It is based on a least-squares type shape comparison with a one to one correspondence.⁹ The Procrustes formula includes translation, rotation, and scaling operations in matching a shape and is shown in Figure 2. The method compares the boundary points on the two shapes with equal number of points.

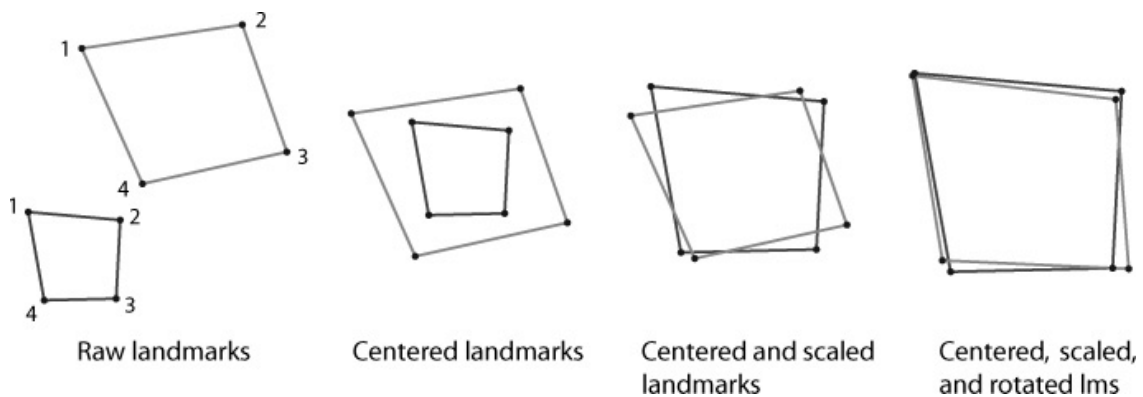


Figure 2: Process of the Procrustes Method in Fitting One Shape to Another¹⁰

2.2.1 Previous Work with Procrustes Method

Procrustes analysis has been used in other applications. Perez-Sala used Procrustes analysis to align postures of athletes in photographs with computer vision.¹¹ This helps the artificial intelligence classify photos more easily. Facial recognition also uses Procrustes analysis in three-dimensions to compare distinguished features and identification. Puente, mentions that Procrustes analysis can be used for matching clusters of data points.¹² Procrustes has also been used in dental studies to study the shape of teeth to find the average shape of a tooth among the general population.¹³ Goodall et al. found a difference in the shape of rats' skulls with nutritional

deficiencies using Procrustes analysis.¹⁴ In this study we will be using Procrustes analysis to compare ACL cross sections to predefined shapes.

2.2.2 Description of Procrustes Formula

Let **A** and **B** correspond to two shapes as represented by matrices of n evenly spaced cartesian boundary points. The number of boundary points, n, is the same for both shapes. Let \mathbf{A}^x and \mathbf{A}^y be column vectors of matrix **A** which correspond to the x and y coordinates of the boundary points, respectively. The boundary points are consecutively ordered based off their location. This is important since the comparison will be a one-to-one point comparison. Similarly let \mathbf{B}^x and \mathbf{B}^y be column vectors of the x and y boundary points of the second shape in the matrix **B**. The matrix **A** will contain the coordinates of what will be called the reference shape. The matrix **B** will contain the coordinates for what is termed the compared shape. The mean values of the x and y components for the two shapes are calculated as $\bar{A}^x, \bar{A}^y, \bar{B}^x,$ and \bar{B}^y , respectively, where \bar{A}^x , for example, is given by equation (2-1).

$$\bar{A}^x = \left[\frac{1}{n} \sum_{i=1}^n A_i^x \right] \quad (2-1)$$

The coordinates in **A** and **B** need to be centered about a common origin so their respective centroids are at the same location. For this, the mean values of the coordinates are subtracted from every coordinate point. The new matrices will be defined as **AO** and **BO** with their respective column vectors $\mathbf{AO}^x, \mathbf{AO}^y, \mathbf{BO}^x,$ and \mathbf{BO}^y . Equation (2-2) shows how these vectors were calculated with subscript i representing the ith row of the column vector.

$$AO_i^x = A_i^x - \bar{A}^x \quad (2-2)$$

$$[AO] = [AO^x, AO^y] \quad (2-3)$$

The sets of coordinates will be normalized for comparison. The normalized coordinate matrices will be termed **ANORM** and **BNORM**.

$$[ANORM] = \frac{1}{\sqrt{\sum_{i=1}^n (AO_i^x)^2 + \sum_{i=1}^n (AO_i^y)^2}} [AO] \quad (2-4)$$

$$[BNORM] = \frac{1}{\sqrt{\sum_{i=1}^n (BO_i^x)^2 + \sum_{i=1}^n (BO_i^y)^2}} [BO] \quad (2-5)$$

The denominator in equations (2-4) and (2-5) is called the Frobenius norm. Now that coordinates have been centered about the origin and normalized, the Procrustes formula can now be used. Now let **R** be the orthogonal transformation matrix that minimizes the sum of squares of the residual matrix **E** in equation (2-6).^{15,16}

$$E = B_{norm}R - A_{norm} \quad (2-6)$$

Let the value g_1 be the sum of squares of **E** shown in equation (2-7). A second condition for **R** is that it is unitary, shown in equation (2-8), where **L** is a Lagrange multiplier matrix of unknown values. To minimize both values, the sum of the partial derivatives were set to 0 in equation (2-9).

$$g_1 = tr(E^T E) \quad (2-7)$$

$$g_2 = tr(L(R^T R - I)) \quad (2-8)$$

$$\frac{\partial g}{\partial R} = \frac{\partial g_1}{\partial R} + \frac{\partial g_2}{\partial R} \quad (2-9)$$

$$\frac{\partial g}{\partial R} = (B_{norm}^T B_{norm} + B_{norm} B_{norm}^T)R - 2B_{norm}^T A_{norm} + R(L + L^T) = 0$$

The matrices $(B_{norm}^T B_{norm})$ and $(L + L^T)$ in equation (2-9) are symmetric.

$$\frac{L + L^T}{2} = R^T B_{norm}^T A_{norm} - R^T B_{norm}^T B_{norm} R = \left(\frac{L + L^T}{2} \right)^T \quad (2-10)$$

Since $(L + L^T)$ and $(R^T B_{norm}^T B_{norm} R)$ are symmetric then $(R^T B_{norm}^T A_{norm})$ is also symmetric from equation (2-10). Therefore, the condition in equation (2-11) must be met.

$$R^T (B_{norm}^T A_{norm}) = (A_{norm}^T B_{norm}) R \quad (2-11)$$

Multiplying equation (2-11) by R on the right and R^T on the left yields equations (2-12) and (2-13) respectively.

$$B_{norm}^T A_{norm} = R (A_{norm}^T B_{norm}) R \quad (2-12)$$

$$R^T (B_{norm}^T A_{norm}) R^T = A_{norm}^T B_{norm} \quad (2-13)$$

Multiplying equation (2-12) by equation (2-13) on the right yields equation (2-14) where both sides of the equation are symmetric.

$$B_{norm}^T A_{norm} A_{norm}^T B_{norm} = R (A_{norm}^T B_{norm} B_{norm}^T A_{norm}) R^T \quad (2-14)$$

Both sides of equation (2-14) have the same eigenvalues. Let $M = B_{norm}^T A_{norm}$.

$$svd\{MM^T\} = R svd\{M^T M\} R^T \quad (2-15)$$

Where $svd\{\}$ is the singular value decomposition function in equation (2-15).

$$svd\{M\} = USV^T \quad (2-16)$$

$$svd\{M^T\} = svd\{M\}^T = VS^T U^T \quad (2-17)$$

\mathbf{U} and \mathbf{V} are unitary orthonormal eigenvectors and \mathbf{S} is the diagonal eigenvalue matrix in equations (2-16) and (2-17). A unitary matrix has the condition that $UU^T = I$. A diagonal matrix has only elements in the diagonal of the matrix as its name suggests. Since the singular value decomposition function is distributive, equations (2-15)-(2-17) are combined to form equation (2-18)

$$(USV^T)(VS^T U^T) = R(VS^T U^T)(USV^T)R^T \quad (2-18)$$

Since \mathbf{U} and \mathbf{V} are unitary and \mathbf{S} is diagonal, equation (2-18) is simplified into equation (2-19).

$$US^2U^T = RVS^2V^TR^T \quad (2-19)$$

In order for equation (2-19) to be true, equation (2-20) must be true as well.

$$R = UV^T \quad (2-20)$$

Once again \mathbf{R} is the transformation matrix mapping **BNORM** to **ANORM**. The eigenvalue decomposition matrix, \mathbf{S} , can be used to calculate the Procrustes distance in equation (2-21).

$$Pd = 1 - tr(S)^2 \quad (2-21)$$

The diagonal values in \mathbf{S}^2 are equivalent to the eigenvalues found in equation (2-22).

$$|MM^T - \lambda I| = 0 \quad (2-22)$$

Where I is the 2 by 2 identity matrix and λ is the eigenvalue. The closer the Procrustes distance is to 0, the closer the fit of the set of coordinates in B matches to the set of coordinates in A and hence the closer the two geometric shapes.

3.0 Methods

For the acquisition of data, the following methods were used. First the specimen was prepared for testing. Then the specimen was placed in a robotic testing system to place the specimen in a precise position. The specimen was laser scanned and the data was converted into a three-dimensional computer model. Cross sections of the model were taken with respect to the axis of the ACL. These cross sections were then compared to predetermined shapes using Procrustes analysis. Procrustes shape analysis was used to compare the fit of five shapes, (ellipse, rectangle, triangle, peanut shape, and kidney shape) to the ACL cross section.

3.1 Specimen Preparation

Ten freshly frozen cadaveric human knees were dissected and the femoral and tibial ends cast in resin.

The ends of the femur and tibia were placed in a six degree of freedom robotic testing system. The coordinate system used is X in the medial-lateral direction of the knee, Y vertical to the ground and Z in the anterior-posterior direction of the knee.

Then a program controlling the robot was used to position the knee so that the forces holding the knee were minimized in order to have the knee in a natural position. The robot determines the passive path of the knee from full extension to 15 degrees flexion. That angle of flexion was found to be the highest in-situ force in the ACL under a quadriceps load.¹⁷

After the robot has acquired the passive path of the intact knee, the knee was removed from the robot for dissection. All tissue and the femoral condyles were removed so that the ACL can be visualized. After dissection, the surgeon marks with a surgical pen the femoral and tibial insertion sites with evenly spaced marks. The marks are shown below in Figure 3.

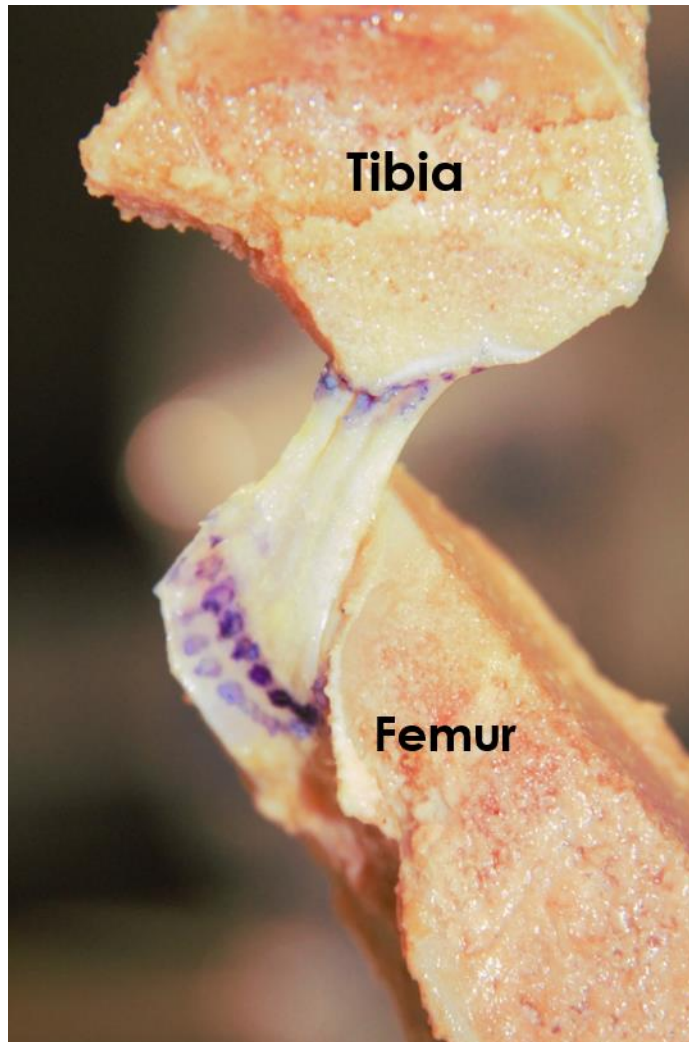


Figure 3: Dissected Knee so that Only ACL, Tibia, and Femur Remain

The specimen was then returned to the robot and placed in the same position of 15 degrees flexion as that of the intact knee.

3.2 Laser Scanning of the Anterior Cruciate Ligament

The laser scanner (Faro, Inc.) interfaces with a solid modelling program (Geomagic, Inc.) to generate three-dimensional computer models of the scanned object. The coordinates of the system were set to X, Y and Z which have been previously defined. Then the ACL insertion sites were then digitally recorded with the laser scanner. The laser scanner has a 1 mm precision in three-dimensional space that matches the precision of the pen used to mark the insertion sites. Twenty points were measured around each insertion site. The laser scanner was then used to scan the ACL including the immediate surrounding bone.

3.3 Analysis of Three-Dimensional Computer Model

3.3.1 Creating the Solid Model

Once the ligament was scanned, the data was converted into a three-dimensional solid model (Geomagic, Inc). Then the model was processed by applying a general smoothness function, removing overlapping elements, and filling any holes in the model.

3.3.2 Defining the ACL Cross Sectional Axis

Before ligament cross sections can be determined, the axis normal to the cross sections must be defined. This was nontrivial because of the tissue's nonuniform geometry. This axis was

chosen to be the vector connecting the centroids of the femoral and tibial insertion sites. To calculate these centroidal positions, the mean value of the coordinate points that were digitized around the border of the insertion sites were calculated.

In order to have cross sections only of the tissue, the regions of the solid model that were bone were removed. This was done by defining two splines around the boundary of the insertion sites and removing elements outside the splines.

After this modification, the planes for the cross sections of the ligament were defined. The planes are perpendicular to the axis of the ACL. To define locations of proximal and distal sections of the ACL, five cross sectional planes were equally spaced across the length of the ligament so that bone was not included in the cross section. Points along the boundary of the cross sections of the tissue at these planes were found in terms of three-dimensional coordinates. Each cross sectional boundary was chosen to have 999 coordinate points.

3.4 Shape Analysis of Ligament Cross Sectional Area

3.4.1 Processing of the Cross Sectional Data

With the collection of n cross sectional boundary data points and the directional vector of the ACL, the three-dimensional coordinates were converted into a set of two-dimensional planar coordinates. For this, the X , Y , and Z coordinate system was transformed using a rotation matrix, in a MATLAB program, for the transformation.

The cross sectional boundary points were input into a n by 3 array, defined as \mathbf{T} with the columns corresponding to \mathbf{X} , \mathbf{Y} , and \mathbf{Z} global coordinates. This is shown in equation (3-1).

$$[T] = [X, Y, Z] \quad (3-1)$$

The transformation matrix, \mathbf{Q} , was computed using the following steps. First, the ACL axis vector was used to define one of the three new base unit vectors. The second base unit was defined as perpendicular to the ACL axis and the global z axis in a direction similar to that of the global x axis. The third base unit vector is defined as the cross product of the first two base unit vectors. The collected directional vector components of the ACL axis, from the three-dimensional model, were listed as x_D, y_D , and z_D . The ACL axis is the transformed Y axis. The vector to be used as the transformed X axis is analogous to the sagittal plane perpendicular to the ACL axis shown in equation (3-2).

$$\vec{v}_x = y_D \hat{i} - x_D \hat{j} \quad (3-2)$$

$$\vec{v}_y = x_D \hat{i} + y_D \hat{j} + z_D \hat{k} \quad (3-3)$$

The X direction vector is converted to a unit vector. The ACL axis vector is already a unit vector. The vectors in new coordinate system can be shown in equations (3-4)-(3-6).

$$\hat{v}_x = \frac{\vec{v}_x}{\|\vec{v}_x\|} \quad (3-4)$$

$$\hat{v}_y = \vec{v}_y \quad (3-5)$$

$$\hat{v}_z = \hat{v}_x \times \hat{v}_y \quad (3-6)$$

The global coordinate system is represented as \mathbf{G} , a 3 by 1 matrix where each row is a three-dimensional vector.

$$[G] = \begin{bmatrix} \hat{g}_x \\ \hat{g}_y \\ \hat{g}_z \end{bmatrix} = \begin{bmatrix} 1 & 0 & 0 \\ 0 & 1 & 0 \\ 0 & 0 & 1 \end{bmatrix} \begin{bmatrix} \hat{i} \\ \hat{j} \\ \hat{k} \end{bmatrix} \quad (3-7)$$

Similarly, the transformed coordinate system is represented as \mathbf{V} .

$$[V] = \begin{bmatrix} \hat{v}_x \\ \hat{v}_y \\ \hat{v}_z \end{bmatrix} = \begin{bmatrix} \frac{y_D}{\|\vec{v}_x\|} & \frac{-x_D}{\|\vec{v}_x\|} & 0 \\ x_D & y_D & z_D \\ \frac{-x_D z_D}{\|\vec{v}_x\|} & \frac{-y_D z_D}{\|\vec{v}_x\|} & \|\vec{v}_x\| \end{bmatrix} \begin{bmatrix} \hat{i} \\ \hat{j} \\ \hat{k} \end{bmatrix} \quad (3-8)$$

From the new matrix and the global matrix, the transformation matrix \mathbf{Q} was constructed where the subscript notation is used to indicate the row of the matrix shown in equation (3-9).

$$\mathbf{Q}_{ij} = \mathbf{V}_i \cdot \mathbf{G}_j \quad (3-9)$$

With this transformation matrix the array \mathbf{T} was converted into \mathbf{T}' , an array of transformed coordinates using the equation (3-10),

$$[T'] = [T][Q^T] \quad (3-10)$$

where \mathbf{Q}^T is the transpose of \mathbf{Q} .

Now the cross sectional boundary points share the same Y value due to the transformation. Since the cross section was now two-dimensional the Y coordinate was removed when storing the points.

After the cross sectional boundary points were converted into two-dimensional data they were normalized for analysis. This includes centering the cross section, ordering them and converting units. For the centralization, the mean value of both coordinates was subtracted from each point. It is important to index the points such that each point is located to its most proximal neighbor. To order the points, a function was created that loops through all the points and finds the point with minimum distance to each one and makes the necessary swaps in the array to place them in order. Folds in the cross section do not affect the ordering since the number of points in the cross section provides enough resolution for the smallest of folds allowed in the model. The units were converted from inches to millimeters.

3.4.2 Creating the Shapes

In order to compare the various shapes to the cross sectional data points, different shapes were constructed. The Procrustes formula needs each shape to have the same number of boundary points as the cross sections (n). In creating each shape, parameters were varied like the eccentricity of an ellipse or the ratio of length to width of a rectangle, to account for different geometries of a shape.

Ellipse

To construct an ellipse, the only parameter varied was the eccentricity. The eccentricity, e , relates the semi major axis, a , and the semi minor axis, b , by the equation (3-11).

$$b = a\sqrt{1 - e^2} \quad (3-11)$$

A 1 by n array of angles between 0 and 2π is established. Then Cartesian coordinates of an ellipse were created with the equations (3-12) and (3-13).

$$X_e = a * \cos(\theta) \quad (3-12)$$

$$Y_e = b * \sin(\theta) \quad (3-13)$$

A MATLAB function called ‘curvspace’ was applied to these points which evenly spaces the points, so that points are not clustered due to angular dependence of the shape. To center the ellipse, the average X_e and Y_e position was subtracted from every point.

Rectangle

To construct a rectangle, the width is the only varied parameter since the length will be scaled by the Procrustes function. To determine the boundary points, polar coordinates cannot be used as was done for the ellipse. For the spacing of points a different method was used since the ‘curvspace’ function cannot be applied to shapes with a discontinuous tangent. This was done by

proportioning the number of points in a linear array by the its relative length. This is shown in the method below.

Let n be the total number of points and L_p and W_p represent the number of points in the length and widths respectively, From the perimeter of a rectangle the following equation was made. $2L_p + 2W_p = n$. The length is dependent on width parameter. $W_p = aL_p$ where a is constant scale factor between 0 and 1. Substituting W_p into the first equation and solving for L_p yields equations (3-14) and (3-15) .

$$L_p = \frac{n}{2(a + 1)} \quad (3-14)$$

$$W_p = \frac{an}{2(a + 1)} \quad (3-15)$$

Because these equations can result in a decimal, each value was rounded up to the nearest integer. To construct the arrays, let L be 1 and $W = aL$. The eight arrays are four arrays of x coordinates and four arrays of y coordinates of the sides.

These sides create a rectangle composed of boundary points that is centered at the origin. This method yields a rectangle that has an even number of total points. To compare the rectangle to a cross sectional boundary having an odd number of points a random point is removed using a random number generator from the rectangle.

Triangle

To determine the boundary points of a triangle, two parameters were altered. These parameters were two of the three angles of the triangle. The third angle is dependent on the values of the other two angles. There are three types of triangles that were constructed, acute, right, and obtuse. All three types of triangles were evaluated. Images of acute and obtuse triangles are shown

in Figure 4 and Figure 5, respectively. An acute triangle being defined as a triangle where all the angles are less than 90 degrees. An obtuse triangle is defined to have one angle greater than 90 degrees. To define the triangle the first angle, θ , was taken to be the angle between the X axis and the first side of the triangle, with counter clockwise being a positive angle, as shown in Figure 4 and Figure 5. The second angle ϕ is the angle between the first side and the second side where the second side connects the first side to the point $x=0$ and $y=1$. The third side is a line on the X axis that goes from 0 to 1. The third angle is $\psi = 180^\circ - (\theta + \phi)$.

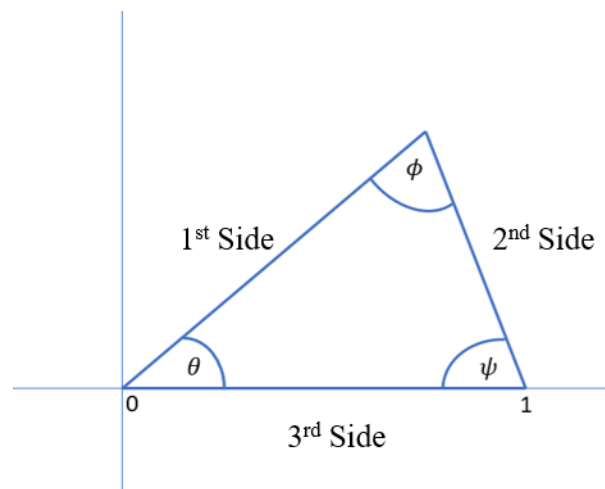


Figure 4: An Accute Triangle with Labeled Sides and Angles

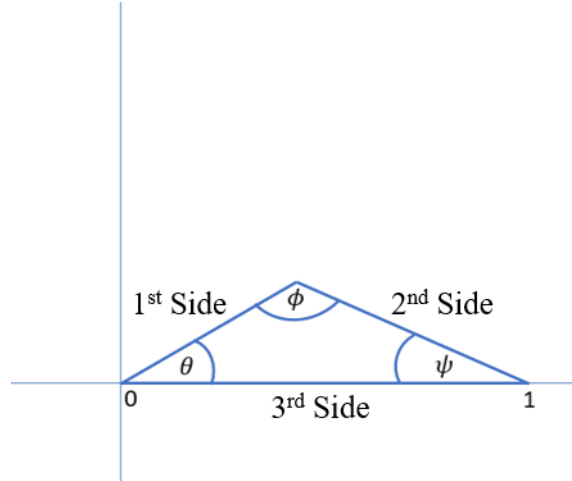


Figure 5: An Obtuse Triangle with Labeled Sides and Angles

The first step in defining the boundary points was to start with converting the first side into its vertical and horizontal components. They were labeled Y_t and X_t respectively. From the trigonometry of an acute triangle, the tangents of θ and ϕ are shown in equation (3-16) and (3-17).

$$\tan(\theta) = \frac{Y_t}{X_t} \quad (3-16)$$

$$\tan(\psi) = \frac{Y_t}{1 - X_t} \quad (3-17)$$

The second equation was substituted for the two known angles in equation (3-18).

$$\tan(\psi) = \tan(180^\circ - \theta - \phi) = -\tan(\theta + \phi) \quad (3-18)$$

When solved for X_t and Y_t in terms of θ and ϕ yields the equations (3-19) and (3-20).

$$X_t = \frac{\tan(\theta + \phi)}{\tan(\theta + \phi) - \tan(\theta)} \quad (3-19)$$

$$Y_t = \tan(\theta) X_t \quad (3-20)$$

The relative length of each side was needed to normalize distance between points.

$$|S_1| = \sqrt{X_t^2 + Y_t^2} \quad (3-21)$$

$$|S_2| = \sqrt{(X_t - 1)^2 + Y_t^2} \quad (3-22)$$

$$|S_3| = 1 \quad (3-23)$$

$$S_t = |S_1| + |S_2| + |S_3| \quad (3-24)$$

The number of points on each side corresponds to the ratio of the side's length to the perimeter of the triangle which is S_t shown in equation (3-24). Since this calculation will end in a decimal like the rectangle, each value was rounded up to the nearest integer.

$$S_{1n} = \frac{|S_1|}{S_t} n \quad (3-25)$$

$$S_{2n} = \frac{|S_2|}{S_t} n \quad (3-26)$$

$$S_{3n} = \frac{|S_3|}{S_t} n \quad (3-27)$$

Then the three sides of the triangle were constructed using x and y coordinate arrays like the rectangle. The first side is simply composed of X_t and Y_t . The second side is composed of Y_t for the y array and the x array is a linear function of the y array shown in equation (3-28).

$$X_2 = \frac{Y_2}{\tan(\theta + \phi)} + 1 \quad (3-28)$$

The third side is composed of a x array from 0 to 1 and a constant y array of 0.

This method can be used to create acute and obtuse triangles, but not right triangles, because the tangent of $\theta + \phi$ is undefined. For a right triangle, the following the vectors were used to describe the three sides of the triangle. The first side had a x array from 0 to 1 with the y array

being the sine of the x array. The second side was an x array with a constant value of 1 and a y array from 1 to 0. Lastly the third side is the same array as the acute and obtuse triangles.

Then with the three sides for any type of triangle, the sides were catenated like the rectangle vectors. Then random points were removed using a random number generator until n points remained. The triangle was then centered about the origin by subtracting the average X and average Y value from each point. Like the rectangle, the points were ordered based on their angle with respect to the origin.

Peanut Shape

For the shape of a peanut, polar coordinates were used. Equation (3-29) was similar to the equation for a Cassini oval, where b^2 is the constant equal to the product of the oval's foci to each point on the oval.¹⁸ The parameter b in equation (3-29) changes the characteristic of the peanut shape. The greater the value of the parameter the more the peanut shape resembles an ellipse. The lower the constant the more pronounced the dimples of the shape appear. When comparing against cross sections, b ranged from 1.4 to 2. If $b < 1.4$, then the dimples will intersect and separate the shape into two parts which was not desired. If $b > 2$, then the peanut shape was entirely convex. This can be shown in Figure 6.

$$r = \sqrt{\cos(2\theta) + \sqrt{\cos(2\theta) - 1 + b^4}} \quad (3-29)$$

Then two vectors were created to construct the shape. Starting first with polar coordinates and then transforming to cartesian coordinates. An array of angles from 0 to 2π with n points was constructed and the r array was a function of θ and b.

$$\theta = [0, 2\pi, n] \quad (3-30)$$

$$r = \sqrt{\cos(2\theta) + \sqrt{\cos(2\theta) - 1 + b^4}} \quad (3-31)$$

Due to the fact that some values of r will be complex, X_p and Y_p will be the real parts of the complex value.

$$X_p = \Re(r * \cos(\theta)) \quad (3-32)$$

$$Y_p = \Re(r * \sin(\theta)) \quad (3-33)$$

As with the ellipse, the function ‘curvspace’ in MATLAB, was used to order these points.

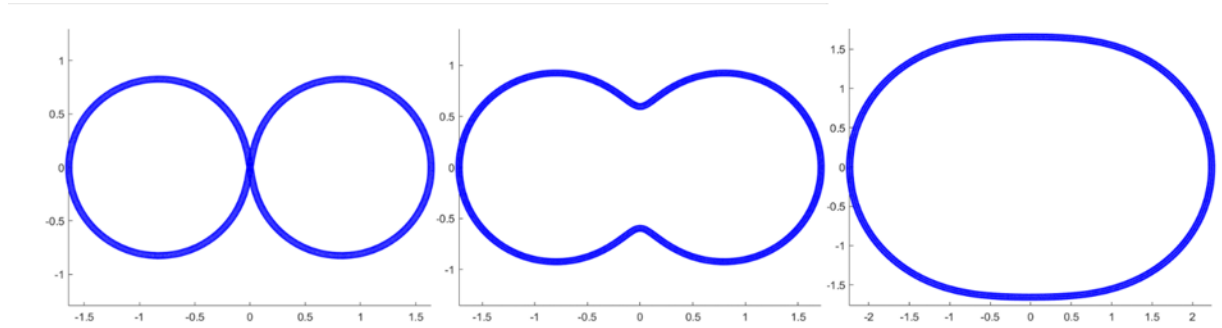


Figure 6: Peanut Shapes with $b = 1.3, 1.4,$ and 2.0 from Left to Right

Kidney Shapes

For a kidney shape, the below polar equation (3-35) was used.

$$\theta = [0, \pi, n] \quad (3-34)$$

$$r = \cos^3(\theta) + \sin^3(\theta) \quad (3-35)$$

Then these polar coordinates were converted into cartesian by the following equations.

$$X_k = r * \cos(\theta) \quad (3-36)$$

$$Y_k = r * \sin(\theta) \quad (3-37)$$

As with the peanut shape and the ellipse, the ‘curvspace’ function to space the points evenly was utilized. Then the average X and average Y value was subtracted from all the coordinates to center the kidney shape about the origin. The kidney shape is shown in Figure 7.

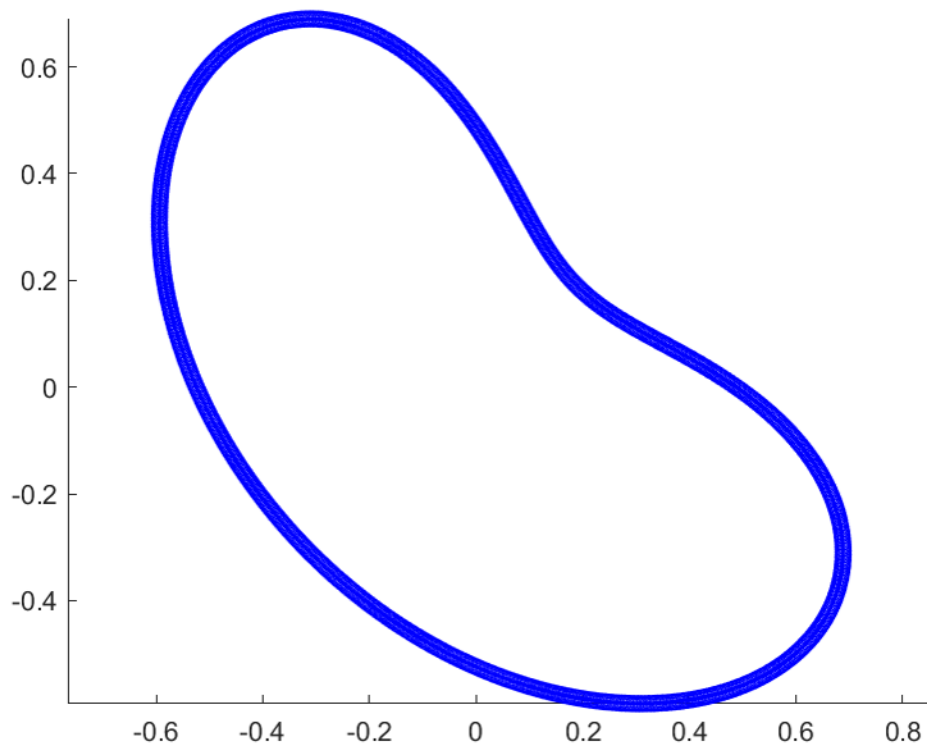


Figure 7: Centered Kidney Shape.

3.4.3 Comparing Defined Shapes to the Cross Sectional Area Point Data

A MATLAB program was used to compare the defined shapes to the boundary point data of the cross sectional area that was measured from the ACL laser scan.

General Comparison

In general, the boundary point data file for a laser scanned cross section was compared to data point file for one of the defined shapes using a MATLAB program and the Procrustes distance is computed in equation (2-21), which has a value between 0 and 1 with 0 being a perfect fit. An iteration is done for different aspect ratios for each shape to compute the minimum Procrustes

distance among all the variations of that shape and the best fit shape, minimum Procrustes distance, is reported.

For example, let a parameter be between 0 and 1. Then the first time through the loop the step of the parameter is adjusted by 0.1. Once the best value is selected like 0.3 then the range is narrowed to adjust the parameter between a range of 0.2 and 0.4 with a step of 0.01.

To verify the computer analysis, the program was used to fit shapes to known boundary point data for exact shapes. The computer program was used to find the best fit for a given shape to exact data for a known shape. For a specific shape the analysis determined the shape parameters and Procrustes distance for the best fit shape. This evaluation yielded that for all of the defined shapes, the exact shape parameter was found and the Procrustes distance had a value of 0. This indicated that the shape fitting algorithm could determine correctly the best fit shape to known shapes.

Next, the specifics will be presented defining the parameters and boundary points for each shape.

Ellipse

An ellipse has only one parameter, the eccentricity. The eccentricity of an ellipse is valued between 0 and 1 and is given by equation (3-38). To fit the shapes of the cross sectional areas of the ACL, the eccentricity was varied between 0.1 and 0.9 but is not a linear correlation between a circle and a line. Therefore, it was needed to adjust our range and steps through the loops.

$$e = \sqrt{1 - \frac{b^2}{a^2}} \quad (3-38)$$

The first loop iterated through eccentricity of 0.1 and 0.9 with steps of 0.1. Letting the best step represented by e_1 .

The second loop iterated through eccentricity values between $e_1 - 0.1$ and $e_1 + 0.1$ with steps 0.01. Letting the best step of this loop be represented by e_2 .

A third loop for the ellipse was created because of the non-linearity in the eccentricity. This loop iterated through $e_2 - 0.01$ and $e_2 + 0.01$ with steps 0.001. This was the final loop through parameters and gave the precise eccentricity of the best ellipse to fit the cross section. The Procrustes function also maps the ellipse onto the cross section so that the scaled semi major axis of the final ellipse was collected. A cross section overlapped with an ellipse is shown below in Figure 8.

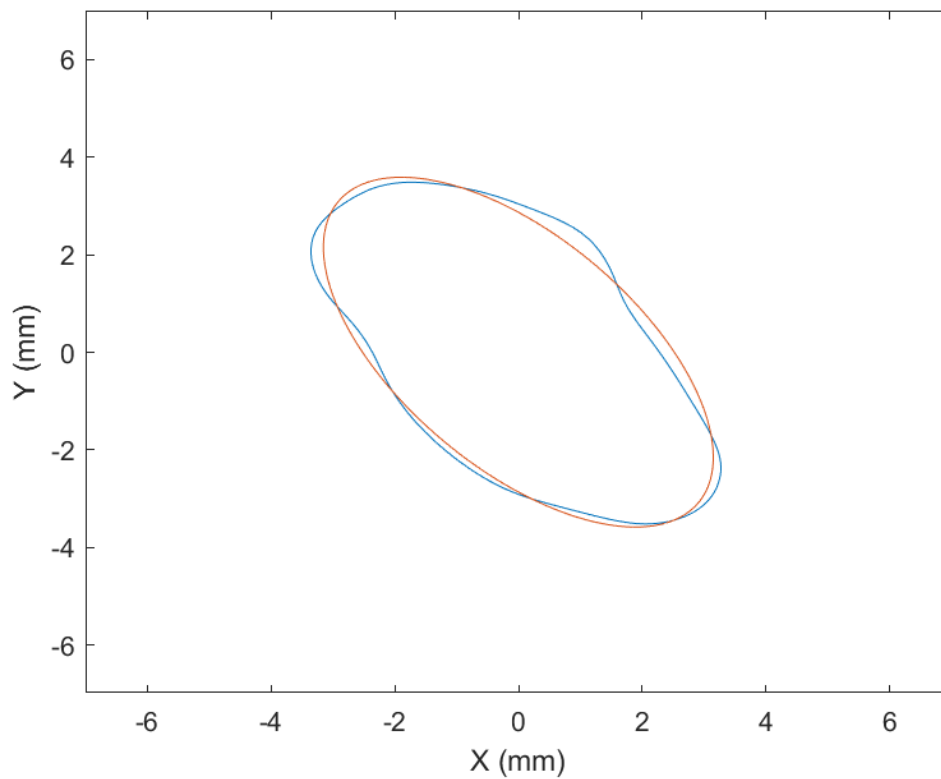


Figure 8: Best Fit Ellipse Compared to the Mid-Level of Sample 5 with Procrustes Distance Equal to 0.0019

Rectangle

The rectangle has only one parameter like the ellipse. This is the ratio between the width the length. $a = \frac{W}{L}$. Since this is a linear relation, the high precision as found in the ellipse is not needed. The first loop iterated through ratio values between 0.1 and 1 with steps of 0.1. As with the ellipse, let a_1 be the best step. The second and final loop iterated through ratio values of $a_1 - 0.1$ and $a_1 + 0.1$ with a step size of 0.01.

From this function the final width and length of the rectangle that best matches the cross section were calculated. A cross section overlapped with the best fit rectangle is shown below in Figure 9.

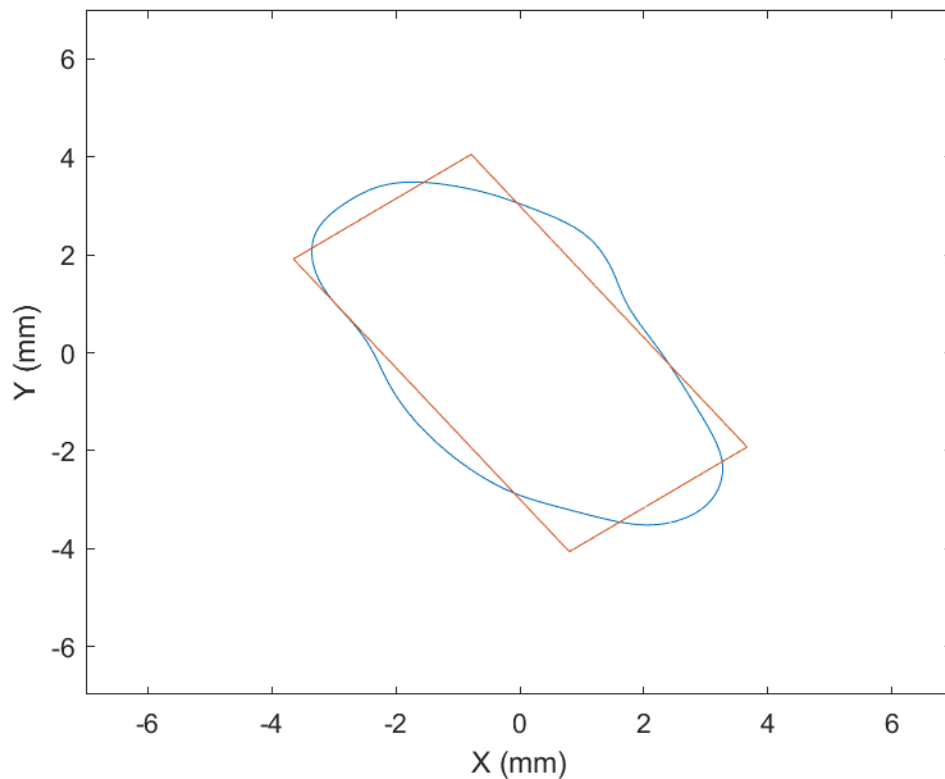


Figure 9: Best Fit Rectangle Compared to Mid-Level of Sample 5 with Procrustes Distance Equal to 0.0129

Triangle

The triangle has two parameters which are the two angles, θ and ϕ , to iterate through. Multiple permutations of angles iterating through both angles were needed.

The first nested loop iterated θ between 10° and 160° with steps of 10° and iterated ϕ between 10° and 160° with steps of 10° . The best step for θ was represented by θ_1 and the best step for ϕ was represented by ϕ_1 .

The second nested loop iterated θ between $\theta_1 - 9^\circ$ and $\theta_1 + 9^\circ$ with steps of 1° . While ϕ was iterated between $\phi_1 - 9^\circ$ and $\phi_1 + 9^\circ$ with a similar step of 1° .

Taken from the triangle comparison, were the final two angles and the scale length which was calculated as the distance to furthest point from the origin. The cross section with the best fit triangle is shown below in Figure 10.

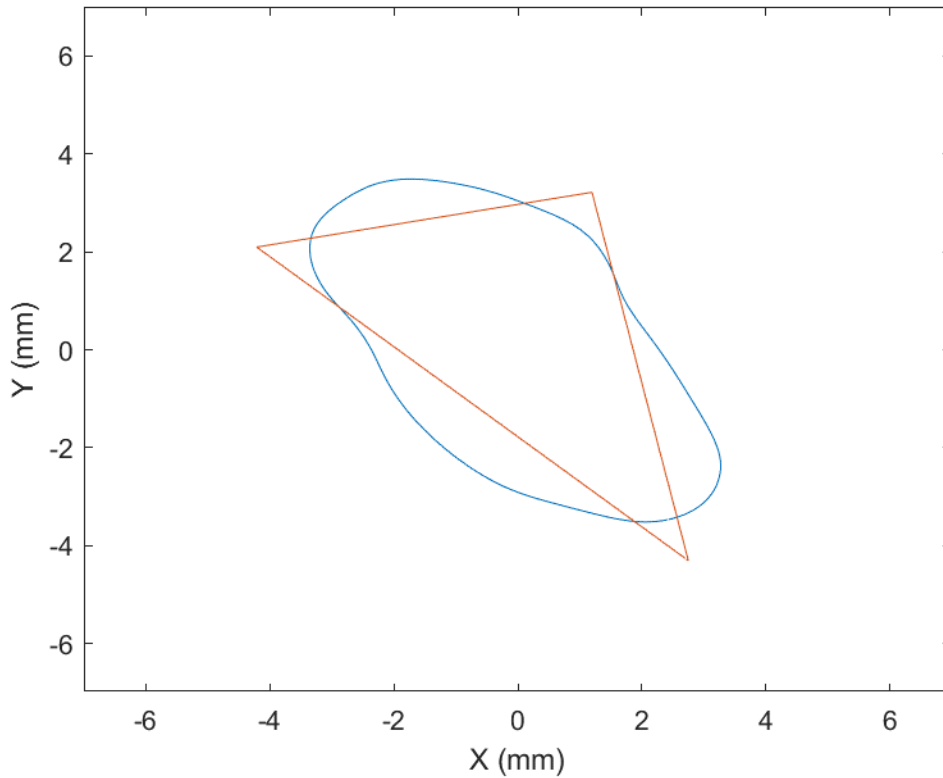


Figure 10: Best Fit Triangle Compared to Mid-Level of Sample 5 with Procrustes Distance Equal to 0.0429

Peanut Shape

The peanut shape has only one parameter b which changes the characteristic dimple of the peanut shape. Discussed earlier, the b that best characterizes the shape is between values 1.4 and 2 which is the range.

The first loop iterated through values of b between 1.4 and 2 with steps of 0.1. The best step was represented by b_1 .

The second and final loop iterated b between $b_1 - .09$ and $b_1 + .09$ with steps of .01. The scale length of the peanut shape and the final value of b were collected. A cross section with the best fit peanut shape is shown in Figure 11.

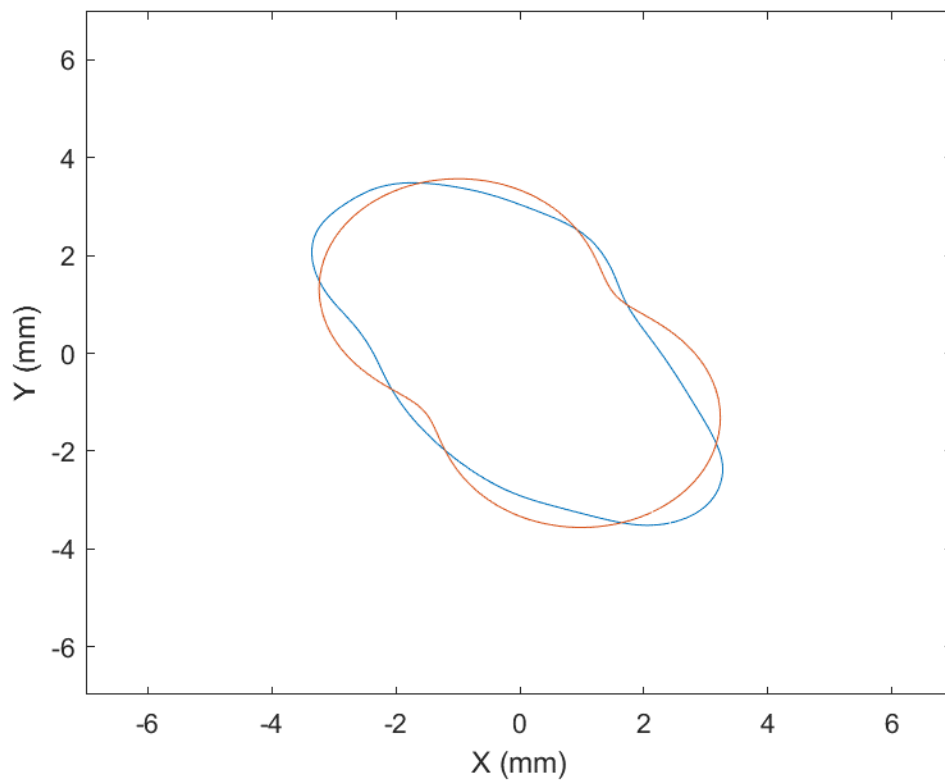


Figure 11: Best Fit Peanut Shape Compared to Mid-Level of Sample 5 with Procrustes Distance Equal to 0.0084

Kidney Shape

The kidney shape has no parameters and therefore is one of the easiest to compare. The scale length information was extracted from the program once it had compared to a cross section. A cross section with the best-fit kidney shape is shown in Figure 12.

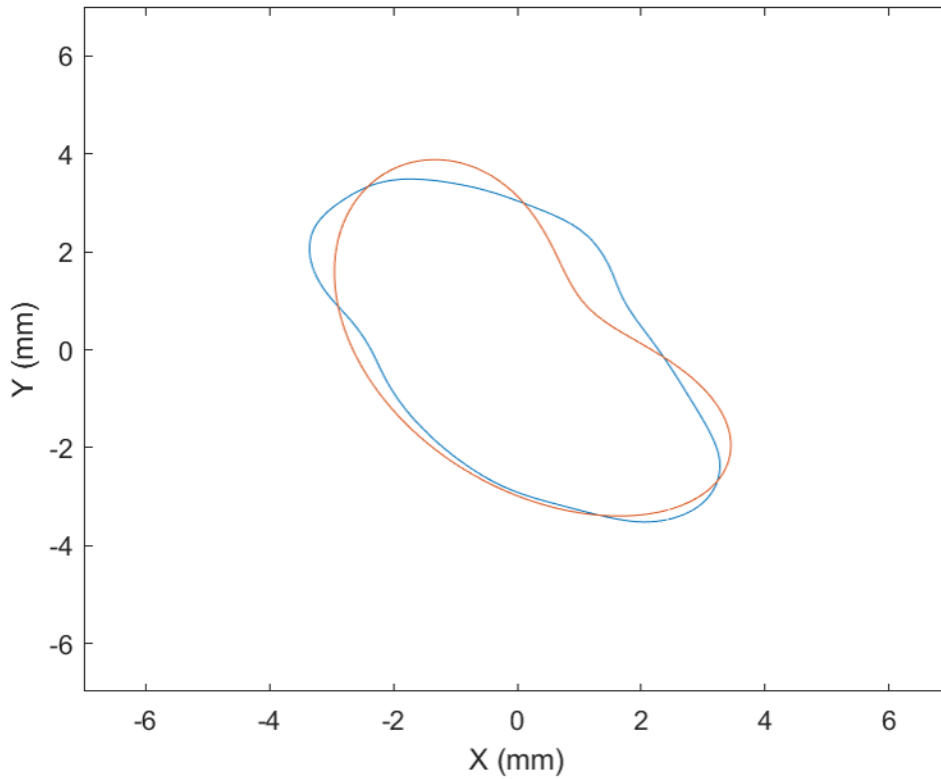


Figure 12: Best Fit Kidney Shape Compared to Mid-Level of Sample 5 with Procrustes Distance Equal to 0.0097

3.4.4 Analysis of the Data

Five different views of the data were analyzed. The first was identifying the best fit shapes for each of the 50 cross sections. Next, the average and standard deviation of the Procrustes distance were calculated for each shape for all cross-sections. Thirdly the best fit shape by level of cross section for all samples. The fourth comparison looks at the best fit shape for one sample

among all the levels. Lastly a view at the difference in distribution of best fit shapes between the mid-level, proximal, and distal cross section was analyzed.

4.0 Results

Five different views were used to quantify the results. First was a comparison of the best shape among all cross sections which over 50% were an ellipse.

The second perspective looked at the average Procrustes distance and standard deviation for each shape where the ellipse again outperformed the other shapes by 7×10^{-4} .

The next comparison related the different levels of the ACL with level 1 corresponding to the cross section closest to the tibia and level 5 closest to the femur. Here is shown a small shift in increasing levels from mostly elliptical shapes to more complex ones like the peanut shape and the kidney shape.

The fourth perspective focused on each specimen to see if the shape was specimen dependent. It can be seen in Table 5 that the 9th specimen was unique in having the best shape be a rectangle for 3 out of the 5 levels.

Finally, the difference between the mid-level (3), and proximal and distal levels (5) and (1) respectively. The proximal and mid-level shared a similar distribution of best shapes, while the distal level differed from both.

The best shape fit for each shape and level is shown in Table 1, which shows the overall results.

Table 1: Best Shape in Each Shape and Level

Sample	Level 1	Level 2	Level 3	Level 4	Level 5
1	Triangle	Ellipse	Ellipse	Peanut	Ellipse
2	Triangle	Ellipse	Ellipse	Triangle	Triangle
3	Ellipse	Ellipse	Ellipse	Rectangle	Kidney
4	Ellipse	Ellipse	Kidney	Ellipse	Ellipse
5	Ellipse	Ellipse	Ellipse	Ellipse	Ellipse
6	Ellipse	Ellipse	Ellipse	Kidney	Peanut
7	Ellipse	Ellipse	Ellipse	Ellipse	Kidney
8	Ellipse	Ellipse	Kidney	Kidney	Kidney
9	Rectangle	Rectangle	Rectangle	Triangle	Triangle
10	Ellipse	Ellipse	Ellipse	Triangle	Rectangle

4.1 Best Fit Shape for Individual Cross Sections

Out of 10 samples with 5 cross sections each making a total of 50 individual cross sections, 29 best fit an ellipse, 5 best fit a rectangle, 7 best fit a triangle, 2 best fit a peanut shape and 7 best fit a kidney shape. This data is given in Table 2.

Table 2: Best Fits for All Cross Sections

Shape	Ellipse	Rectangle	Triangle	Peanut	Kidney	Total
Best Fits	29	5	7	2	7	50
Percent	58%	10%	14%	4%	14%	100%

It is of interest to point out that 3 out of the 5 cross sections that best fit a rectangle were all from the same sample. This sample also had a cross sectional area more than twice that of any other sample.

4.2 Best Fit Shape for All Cross Sections

The average value of the Procrustes distance (PD), was taken for each shape fit for the fifty different cross sections and given in Table 3.

Table 3: Average Procrustes Distance for All Shapes over All Cross Sections

Shape	Ellipse	Rectangle	Triangle	Peanut	Kidney
Average PD 10^{-3}	14.096	21.015	28.393	26.591	22.937
Standard Deviation of PD 10^{-3}	12.41	10.446	10.787	13.807	14.453

In which case the best average shape was the ellipse.

4.3 Best Fit Shape by Cross Section for All Specimens

Looking at the best shape among the level yielded Table 4.

Table 4: Best Shape for Each Level

Level	Ellipse	Rectangle	Triangle	Peanut	Kidney
1	7	1	2	0	0
2	9	1	0	0	0
3	7	1	0	0	2
4	3	1	3	1	2
5	3	1	2	1	3

The ellipse was the better fit for Levels 1,2 and 3 for 70%,90%, and 70% of the samples. Levels 4 and 5 have a mix of shapes. A general trend seen was that the peanut shape and kidney shape rarely fit the first 3 levels but fit some samples in the 4th and 5th level.

4.4 Best Fit Shape for One Specimen Amongst All Levels

When looking at each specimen as in Table 5 we see the following results.

Table 5: Best Shapes for Each Sample

Sample	Ellipse	Rectangle	Triangle	Peanut	Kidney
1	3	0	1	1	0
2	2	0	3	0	0
3	3	1	0	0	1
4	4	0	0	0	1
5	5	0	0	0	0
6	3	0	0	1	1
7	4	0	0	0	1
8	2	0	0	0	3
9	0	3	2	0	0
10	3	1	1	0	0

The ellipse is the best shape for the individual sample for 70% of the samples. Sample 9 being an exception to other samples by not having any of the 5 cross sections have a best fit of an ellipse.

4.5 Mid-Level Cross Section vs Distal and Proximal Cross Sections

The proximal cross section which is closest to the femur is similar to the mid-level cross section. The distal cross section which is closest to the tibia has a different distribution of shapes than the proximal cross section and the mid-level cross section. This can be shown in Table 6.

Table 6: Comparison of Mid-Level Cross Section vs Proximal and Distal Cross Sections

Level	Ellipse	Rectangle	Triangle	Peanut	Kidney
1	7	1	2	0	0
3	7	1	0	0	2
5	3	1	2	1	3

5.0 Discussion

The method of Procrustes method was compared against three other methods of shape analysis. Then applications of this study were discussed. Finally, the overall limitations of this study primarily lied in the scanning and modeling of the samples.

5.1 Comparison

Finite element scaling analysis (FESA) is used in three-dimensional shape analysis by fitting elements between landmarks. The advantage of FESA is the ability to locate morphometric differences in different objects. FESA does not have a good statistical measure though. It is best used for comparisons between large number of samples but not as precise in comparing detailed measurements between a few samples. FESA has been used to compare craniums of primates in anthropology in a variety of studies.¹⁹ FESA requires the use of landmarks and this study does not have defined landmarks.

Thin plate splines or TPS is similar to the idea of mapping a terrain function to a two-dimensional set of points to minimize the “bending energy” of the function between points.¹⁹ The bending energy criteria provides a non-symmetric fitting function. Therefore, the bending energy to morph shape A into shape B is different than the bending energy to morph shape B to shape A. This method is not applicable to this study since this study needs to standardize the quantity of shape similarity.

Euclidean distance matrix analysis (EDMA) uses the length between each landmark of a shape to compare different shapes. The advantage of EDMA is that it is able to locate the specific landmark locations that are most distinct between two shapes. The downside of EDMA is that the process of finding the featured landmarks becomes difficult with large number of landmarks.¹⁹ EDMA has the same limitation as FESA in that it require landmarks.

Procrustes analysis has a strength when processing a large number of boundary points. A set back of Procrustes analysis is that it treats every point in a shape with equal importance since the one-to-one comparisons are not weighted. This can lead to non-important features to outweigh the main features simply because there are more of them. An example of a important feature would be a sharp corner like that in a triangle and rectangle. If the Procrustes analysis is not used on equally spaced points the function will yield inconsistent results.²⁰This was why ordering and spacing the points was crucial for the samples and shapes.

While Price et al. and Harner et al. studied the area of the ACL cross section⁴ and ACL footprint⁷ respectively, they did not fit standard shapes to cross sections of the ACL.

5.2 Application

The results from this study can give information on constructing grafts that more closely resemble the shape of the native human ACL. In the future graft sizers with various shapes could be constructed and methods to form non-circular bone tunnels could be devised.

This method of analysis can also be used to study other biological tissues including ligaments, bones, and muscles. It can also be utilized to compare shapes of non-biological objects.

This method can help remove subjective bias when classifying shapes and add an objective measurement of best fit.

5.3 Limitations

This study was not without its limitations. First of all, the sample size and age range are not ideal. This is the case for most cadaver studies.

There are some limitations to the scanning method as well. First of all, the scanner does poorly when detecting concavities with a large depth with respect to the surrounding surface. For this reason, parts of the scans that are near the femoral insertion have a tendency to not be fully rendered. The second limitation is that the combination of the robot's arm and the flexibility of the laser scanner make some angles of scanning impossible leaving imperfections in the model that had to be smoothed in processing. The third limitation of the scanner is that it has trouble connecting sharp vertices. In some cases, the two edges that come to meet end up have an overlap. The overlap had to be removed.

There are computational limits as well. Due to computing time, a precision for the parameter has to be made to optimize accuracy and computing time. Since the function of the Procrustes distance is dependent on shape parameters, the precision in first iteration may not be high enough to determine the global best fit shape parameters. The loop of localized iterations was used to reduce the overall computing time.

6.0 Conclusion

From the results in the previous section, the shape of the ellipse outperformed all other shapes. There will be sequential work on this topic involving kinematic testing, new shapes, and other anatomical structures.

6.1 Conclusion

The ellipse has the best fit to a majority of the cross sections. The peanut shape was shown to have the least number of best fits at 2 out of 50 cross sections. It is recommended that clinicians use an elliptical cross section as a graft in ACL reconstruction to more closely resemble the intact ACL

6.2 Future Work

Future endeavors will include scanning more specimens and under kinematic loading including anterior tibial translation, and interior/exterior rotation.

Future work will entail looking at different shapes that were presented in this project like a crescent moon or 'C' chape. Using Procrustes analysis on other ligaments and biological structures can find the best shape fit for their respective geometries'.

Bibliography

1. Evans, S., Shaginaw, J. & Bartolozzi, A. Acl reconstruction - it's all about timing. *Int. J. Sports Phys. Ther.* **9**, 268–73 (2014).
2. Fujimaki, Y. *et al.* Quantitative in Situ Analysis of the Anterior Cruciate Ligament. *Am. J. Sports Med.* **44**, 118–125 (2016).
3. Edwards, A., Bull, A. M. J. & Amis, A. A. The attachments of the anteromedial and posterolateral fibre bundles of the anterior cruciate ligament : Part 1: Tibial attachment. *Knee Surgery, Sport. Traumatol. Arthrosc.* **16**, 29–36 (2008).
4. Price, T. M. The Morphometric Properties of the Anterior Cruciate Ligament. (University of Pittsburgh, 2020).
5. Freedman, K. B., Glasgow, M. T., Glasgow, S. G. & Bernstein, J. Anterior Cruciate Ligament Injury and Reconstruction Among University Students. *Clin. Orthop. Relat. Res.* **356**, 208–212 (1998).
6. Moore, L. Anatomy Of The Knee: An Introduction To The ACL. *Chicago Heal.* **1**, 1–2 (2017).
7. Harner, C. D. *et al.* Comparative study of the size and shape of human anterior and posterior cruciate ligaments. *J. Orthop. Res.* **13**, 429–434 (1995).
8. Lipman, Y., Al-Aifari, R. & Daubechies, I. The continuous Procrustes distance between two surfaces. *ArXiv* **1**, 1–21 (2011).
9. Stegmann, M. B., Gomez, D. D., Plads, R. P. & Lyngby, D.-K. A Brief Introduction to Statistical Shape Analysis. *Informatics Math. Model. Tech. Univ. Denmark* **15**, 1–15 (2002).
10. Mitteroecker, P. & Huttegger, S. M. The Concept of Morphospaces in Evolutionary and Developmental Biology: Mathematics and Metaphors. *Biol. Theory* **4**, 54–67 (2009).
11. Perez-Sala, X., De la Torre, F., Igual, L., Escalera, S. & Angulo, C. Subspace Procrustes Analysis. *Int. J. Comput. Vis.* **121**, 327–343 (2017).
12. Puente, J. Distances and algorithms to compare sets of shapes for automated biological morphometrics. (Princeton University, 2013).
13. Robinson, D. L., Blackwell, P. G., Stillman, E. C. & Brook, A. H. Planar Procrustes analysis of tooth shape. *Arch. Oral Biol.* **46**, 191–199 (2001).

14. Goodall, B. C. Procrustes Methods in the Statistical Analysis of Shape. 285–321 (1991) doi:10.1111/j.2517-6161.1991.tb01825.x.
15. Schonemann, P. H. A Generalized Solution of the Orthogonal Procrustes Problem. **31**, (1966).
16. Akca, D. Generalized Procrustes Analysis and its applications in Photogrammetry. (2017).
17. Li, G. *et al.* The importance of quadriceps and hamstring muscle loading on knee kinematics and in-situ forces in the ACL. *J. Biomech.* **32**, 395–400 (1999).
18. Gibson, K. The Ovals of Cassini. (2007).
19. Richtsmeier, J. T., Cheverud, J. M. & Lele, S. Advances in Anthropological Morphometrics. *Annu. Rev.* **21**, 283–305 (1992).
20. Kent, B. J. T. & Mardia, K. V. Consistency of Procrustes Estimators. 281–290 (1997).